ELSEVIER

Journal of Chromatography A, 702 (1995) 69–80

JOURNAL OF CHROMATOGRAPHY A

Estimating plate heights in stacked-membrane chromatography by flow reversal

D. Keith Roper[a,*], Edwin N. Lightfoot[b]

[a]*Merck Research Laboratories, P.O. Box 4 WP16-121P, Sumneytown Pike, West Point, PA 19486, USA*
[b]*Chemical Engineering Department, University of Wisconsin, 1415 Johnson Drive, Madison, WI 53706, USA*

Abstract

A novel method to quantitatively evaluate chromatographic separation performance is presented. Distortion of effluent profiles by non-uniform flow is eliminated by reversing flow direction during the experiment. A semiempirical approach accounts for extracolumn effects on peak shape. Effluent profiles are fitted to a closed-form mathematical description of the experiment to estimate plate height values. Plate heights obtained from two stacked-membrane columns decrease from 3.3 μm at 0.52 cm/min to 0.59 μm at 3.8 cm/min, in agreement with dispersive theory. Performance estimates based on moments or bandwidth measurement are less reliable than this method when non-uniform flow or extracolumn effects are significant.

1. Introduction

The purpose of this work has been to measure the separation capability of stacked-membrane chromatography. Reliance upon chromatography as a preparative tool is growing rapidly, particularly in biotechnology [1,2] and in the pharmaceutical [3,4] industry. This has motivated several recent chromatographic developments: efficient perfusive [5,6] and hyperdiffusive [7] column packings, novel polymeric stacked-membrane [8] and chromarod [9] adsorptive geometries, and improved counterflow [10,11] and recycle [12] operating modes.

Stacked-membrane chromatography seems well suited to the demands of preparative biochromatography. Stacked-membrane column residence times are short and bed volumes are small [13]. This counteracts protein degradation by proteolysis and denaturation which increases with processing time [14]. It also increases throughput, reducing the requirement for expensive solvents and tankage common to large-scale chromatography [15].

Stacking multiple membranes in series averages variations in porosity and membrane thickness which may compromise separation performance of single sheets [16]. Stacking also increases bed capacity. Consequently, the performance of existing devices is sufficient to resolve many proteins by informed selection of differential migration and differential elution or "on–off" strategies [17]. Stacked membrane separations of model protein systems are comparable to similar high-pressure liquid chromatographs [18] without requiring high-pressure columns, peripherals or pumps. Preparative stacked-membrane separations maintain laboratory-scale protein purity at high throughput when scaled up with respect to flow-rate and mass loading [19].

* Corresponding author.

0021-9673/95/$09.50
SSDI 0021-9673(94)01068-4

On the other hand, reported measurements of stacked-membrane efficiency vary over nearly two orders of magnitude. Plate height values are compared in the Van Deemter plot [20] in Fig. 1. Plate height [21], which measures effluent bandwidth, increases as resistances to mass transfer from convective dispersion, intraparticle diffusion, boundary layer phenomena, and adsorption in conventional columns become large.

One possible explanation for the variation in Fig. 1. is that plate height completely characterizes band broadening of *symmetric* Gaussian line shapes [22]. Chromatographic systems with a linear adsorption isotherm, constant equilibrium distribution coefficient and concentration-independent transport properties exhibit Gaussian effluent curves whose plate heights equal the ratio of effluent-peak variance to the column length [23,24]. In contrast, stacked-membrane effluent profiles obtained by Raths and by Gerstner were visibly skewed.

It is also likely that different estimation methods contributed to the range of estimated plate heights. Accurate plate height estimates are obtained by fitting time-domain effluent profiles to an appropriate description [25]. This avoids errors from extracolumn effects, noise, baseline drift, tail truncation and peak skewness which undermine methods relying on tangents, moments, or isolated points on a curve.

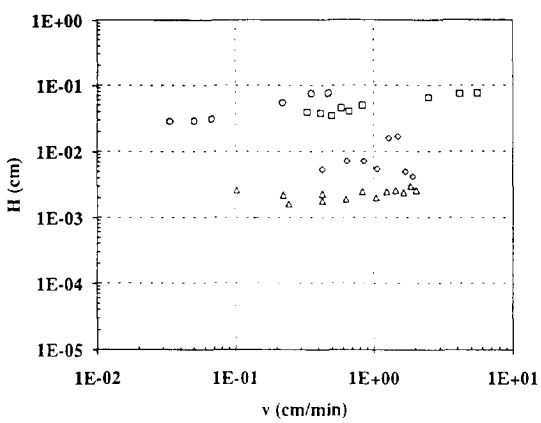

Fig. 1. Plate heights estimated from stacked-membrane effluents. Frey et al. [27] used the experimental method of moments to analyze two stacks of 600 μm poly(vinyl chloride) membranes: 10 mm $L \times 25$ mm I.D. (○) and 50 mm $L \times 25$ mm I.D. (□). Raths [42] fitted effluent profiles from 120-μm regenerated cellulose membranes to an exponentially modified Gaussian: 5 mm $L \times 17$ mm I.D. (◇). Gerstner [19] used an unreported method to analyze stacks of 120-μm regenerated cellulose membranes: 10 mm $L \times 28$ mm I.D. (△).

Finally, reported plate heights, H, are at least ten times greater than values anticipated by an order-of-magnitude analysis of microscopic transport rate processes: intraparticle diffusion is eliminated in ideal stacked membranes by derivatizing adsorptive sites on surfaces of membranes permeated by interconnecting flow-through pores. Boundary-layer fluid-phase mass transfer is negligible as Nusselt numbers in these systems are well above the lower limiting value of 4 [26]. These approximations suggest H in linear, non-adsorbing systems reduces to $H = 2\epsilon/v$ where ϵ represents Fickian convective dispersion. Stacked-membrane chromatography is typically operated such that $H \approx 2D_f/v$ (see Section 2) where D_f is the effective solute diffusivity in unbounded solution. For proteins in stacked membranes, $D_f \approx 5 \cdot 10^{-7}$ cm^2/s and $v \approx 1$ cm/min so that $H \approx 1$ μm.

Three practical questions arise from our observations: (1) How is stacked-membrane plate height accurately measured? (2) What are plate heights of existing stacked-membrane devices? (3) Can commercially available stacked membranes achieve theoretically anticipated efficiencies? We address these issues, beginning with a conceptual description of fundamental mass transport in stacked membranes. Using this description we propose a novel, unambiguous method for determining stacked-membrane efficiencies. We derive analytic expressions, apparently new, which describe the proposed experiment. These expressions allow prediction of separation performance in the presence of significant extracolumn broadening and non-uniform flow.

2. Theory

Two principal, contrasting hypotheses of chromatographic transport in stacked-membrane beds have been examined by previous inves-

tigators: one-dimensional plug flow on the one hand, and two-dimensional unit-cell potential flow on the other. Each proposes a fundamentally different velocity distribution in the porous bed. As a result, broadening in stacked-membrane effluent curves has been attributed to substantially different sources.

After comparing the attributes of these descriptions, we originate a straightforward experimental approach to distinguish between them. Description of this experiment in simple, analytical terms allows separation efficiency in stacked membranes to be characterized.

2.1. Dispersed plug flow in stacked membranes

Consider first a constant, uniform velocity distribution, v, which results from one-dimensional, plug flow parallel to the stacked-membrane axis [13,16,27–29]. A mean particle diameter, $D_p = 3/2d_p(1-\epsilon_b)/\epsilon_b$ in the membrane bed is estimated from its average pore size, d_p, and bulk porosity, ϵ_b [30]. Consequently, a stacked-membrane analogue of the familiar one-dimensional equations of chromatography [31,32] may be derived. Analytic solutions to this equation set are available for numerous special cases [33] including non-linear adsorption [34] and gradient elution [35]; computational solutions are required for more general evaluation of non-linear effects [36] including sample overloading [37].

To determine whether assuming uniform velocity adequately characterizes stacked membranes, a lumped-parameter, asymptotic solution to pseudocontinuum chromatographic equations [38] simplified for non-adsorbing conditions is sufficient. This dispersed plug flow solution anticipates fluid-phase solute concentration distribution c_f from a sharp-pulse input of solute mass m_0 will be a Gaussian function of axial coordinate z when time t is treated as a parameter:

$$c_f(z,t) = \frac{m_0 u}{A\epsilon_b\sqrt{2\pi H z_0}} \cdot \exp\left[\frac{-(z-z_0)^2}{2Hz_0}\right] \qquad (1)$$

The mean solute position, $z_0 \equiv uvt$, is proportional to both the interstitial fluid velocity, v, and the fraction of solute in the moving fluid phase at long times, $u \equiv \alpha\epsilon_b/[\alpha\epsilon_b + (1-\epsilon_b)]$. The column cross-sectional area is A. Subscripts f and b refer to the moving fluid and stationary bulk phases, respectively. The bulk phase consists of derivatized membrane of ideally zero porosity.

The plate height relation for one-dimensional dispersed plug flow in stacked membranes reduces to $H = 2\epsilon/v$, neglecting intraparticle diffusion and fluid-phase mass transfer (see Section 1). This indicates band broadening is due solely to micro-scale fluid-phase mixing phenomena which constitute convective dispersion. These include mixing by solid obstructions to flow, incomplete connectivity, eddies, recirculation from regional pressure gradients, and diffusion [39]. Broadening which results from micro-scale mixing processes is entirely *irreversible*.

The Fickian convective dispersion coefficient is available from Koch and Brady's [40] analysis of ambient, creeping flow in random configurations of fixed spheres which constitute a low fraction of total volume. For a diffusion Peclet number, $Re \cdot Sc \equiv D_p v\epsilon_b/D_f$, greater than unity, they proposed

$$Pe_\epsilon^{-1} = \frac{3}{8}\cdot\epsilon_b + \frac{\pi^2}{12}\cdot\epsilon_b(1-\epsilon_b)\ \ln\left(\frac{Re\cdot Sc}{2}\right) + \frac{\epsilon_b}{Re\cdot Sc} \qquad (2)$$

$$Pe_\epsilon \equiv \frac{vD_p}{\epsilon}$$

It is evident that broadening in dispersed plug flow *changes with velocity*.

The effluent profile indicated by Eq. 1 approaches Gaussian form in time when evaluated at the column exit as the number of column plates, N, becomes large. This distribution is characterized entirely by its first two temporal moments. Consequently, broadening attributed to dispersed plug flow is *distributed symmetrically* around a mean residence time, $\bar{t} = NH/uv$ with a variance of $s^2 \equiv \bar{t}H/uv$. Scaling the variance by the residence time gives the plate number, $N = \bar{t}^2/s^2$.

These natural outcomes from a constant uniform velocity distribution in stacked-membrane chromatography are summarized in Table 1.

Table 1
Dispersed plug flow vs. non-uniform potential flow in stacked membranes

	One-dimensional plug flow	Two-dimensional potential flow
Plate height	$2\epsilon/v$	$c^2/3b$[a]
Plate height value	ca. 1 μm	ca. 1 mm
Broadening	Dispersive	Mechanical
Broadening reversible	No	Yes
Flowrate-independent plate height	No	Yes
Peak shape	Symmetric about $\bar{t}$	Asymmetric

[a] Plate height for single unit cell.

2.2. Planar potential flow in stacked membranes

Now consider a non-uniform, velocity, $v(\Phi,\Psi)$ distributed along potential function, Φ, and stream function, Ψ, coordinates corresponding to two-dimensional potential flow [30] in *unit cells* of a stacked membrane, as sketched in Fig. 2. Balzereit [41] and Raths [42] postulated that distributor channels introduce fluid into such planar flow cells which parallel the column axis. Two ratios of characteristic lengths describe the unit-cell geometry: b/c, where b is the bed height and c is the distance between adjacent distribution channels; and d/c, where d is the channel width.

Numerical solution by discretization along a scaled Φ coordinate and quadrature in a scaled Ψ coordinate yielded unit-cell effluent profiles which were skewed at low flow-rates. Effects of convection as well as radial and axial diffusion were assessed in these computation. Numerical instability precluded calculation of effluent profiles at flow-rates typical of stacked-membrane operation. But numerical estimates of the effective number of theoretical plates in a unit cell $N_{\text{eff}} = \bar{t}^2/s^2$ (the ratio of first to second central temporal moment) reached an asymptotic value at operational flow-rates for each unit cell geometry. Broadening in effluent from non-uniform, planar unit-cell flow in stacked membranes is *independent of flow-rate*.

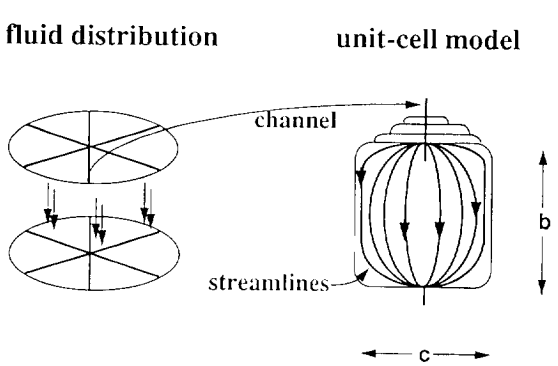

Fig. 2. Two-dimensional potential flow in unit cells of a stacked membrane. Distributor channels etched into distributor endcaps of a stacked-membrane column may introduce fluid into planar flow cells of width c and height b which lie parallel to the axis of the bed [41]. Streamlines are lines of constant velocity.

Flow-rate-independent broadening implies diffusive effects are small relative to convection in non-uniform, unit-cell flow. In other words, band broadening arises entirely from the distribution of residence times corresponding to flow at differing rates along different streamlines, which are lines of constant velocity (see Fig. 2). The geometry of each unit cell —determined by the mechanical structure of the distributors and membrane cross-section— governs its distribution of streamlines. Hence, a potential-flow description of stacked membranes suggests bandwidths have a purely *mechanical* origin.

Broadening dominated by convective residence time differences in stacked membranes is *reversible*, in the sense that a narrow band of tracer particles initially perpendicular to the flow direction will reconverge if the direction of flow is suddenly reversed a short time later.

Negligible diffusion also justifies approximating potential flow in each unit cell by an analytic complex potential [43]. This provides a continuous analytical function for velocity, $\boldsymbol{v}(\Phi,\Psi)$ from which estimates of the first, $\langle t\rangle Q/c^2 \approx b/2c$, and second, $\langle t\rangle^2 Q^2/c^4 \approx (b/2c)^2$, scaled temporal moments can be made [44]. The unit-cell scaled efficiency, $N_{\text{eff}} \approx 3(b/c)^2$ is determined by its geometry.

Stacked-membrane effluent profiles have been calculated by superposing residence time densities of successive unit cells of different geometry, each weighted by the volume fraction of total flow which travels through it [45]. In the MemSep 1000, for example, radial channels distribute flow into successive unit cells whose d/c and b/c decrease to about 0.02 and 0.50 at the periphery of the membrane stack, respectively. Such profiles are *skewed*: tailing in the line shape is similar to measured effluent profiles although the peak is relatively sharp. Plate heights from these profiles by moments analysis are on the order of a millimeter.

Outcomes from non-uniform, two-dimensional potential flow in stacked-membrane chromatography are listed for comparison with dispersed plug flow in Table 1.

2.3. Extracolumn dispersion

Extracolumn contributions to broadening in stacked-membrane effluent profiles are also significant. As stacked-membrane column volume decreases to the same order of magnitude as the volume of injection valves, tubing, adaptors and other peripheral plumbing, it confounds discrimination between dispersed plug flow and planar potential flow by effluent analysis more severely.

Numerical analysis is necessary to rigorously determine extracolumn dispersion at Peclet numbers (ca. 10^6) and times (ca. 0.01 s) typical of stacked-membrane operation, even in short straight [46] or curved [47] cylindrical tubes. And the apparent complexity of peripheral plumbing produces effluent profiles unlike those from simple tubes [48,49].

We adopt, instead, a semiempirical approach to estimate extracolumn effects in stacked-membrane systems. Effluent profiles from peripherals at each experimental condition are fit to an exponentially modified Gaussian (EMG) form [50] which represents the convolution of plug flow and continuous stirred-tank reactors. Results are illustrated in Fig. 3 for precolumn peripherals. Fitted parameters are the mean residence time, $\bar{t}$ and variance σ^2 of the underlying Gaussian and the stirred-tank time constants, τ.

2.4. Reversed-flow analysis of stacked membranes

Fundamental distinctions between dispersion in plug flow and residence-time distribution in planar potential flow preclude attributing broadening caused by either source to the other. In order to distinguish their relative contributions, consider reversing the flow direction at half the mean residence time after a injecting a sharp pulse of tracer at the column inlet. Detect

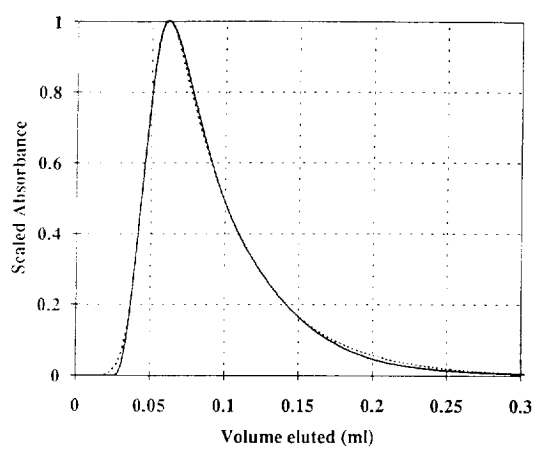

Fig. 3. Effluent from precolumn tubing, fittings and injection valves (solid line) for a MemSep 1000 compared with an exponentially modified Gaussian fit (dashed line). A 20-μl sample of 2.5 mg/ml cytochrome c was eluted at 2 ml/min; absorbance was measured at 280 nm in a 10-mm flow cell. Fitted parameters are the mean residence time, $\bar{t}_r = 0.047$ min and standard deviation $\sigma_r = 0.0097$ min of the underlying Gaussian and the stirred-tank space time, $\tau_r = 0.047$ min.

the cup-mixed effluent profile at the column inlet as it emerges.

Particles convected by different velocities along different streamlines will reconverge following flow reversal. At the detection point, broadening produced by all macroscopically non-uniform flow, including planar potential flow, will disappear. Meanwhile, particles dispersed axially along a streamline by irreversible mixing processes will continue dispersing after flow reversal. The net dispersion of particles traveling at the mean velocity is identical, whether detected at the inlet after flow reversal or detected at the outlet after traversing the entire length of a column symmetric about its midplane.

Aside from large flow non-uniformities, a ratio of operational membrane velocity to macromolecular diffusion coefficient, $(1\ \mathrm{cm/min})/(5 \cdot 10^{-7}\ \mathrm{cm^2/s}) \approx 0.3\ \mu\mathrm{m}$, suggests broadening arising from dispersion across streamlines will generally be small. Dispersion coefficients of streamlines with velocities above about 1 cm/min will be comparable, as Eq. 2 suggests (see also Fig. 8).

Qualitative evidence of non-uniform flow is indicated by broadening in forward effluent bands which is more severe than comparable reversed-flow results, provided upstream and downstream peripherals in each experiment are identical. Estimating the variance of a reversed-flow effluent profile promises an unambiguous, quantitative measure of stacked-membrane separation potential after accounting for extracolumn effects.

A symbolic representation of the components which describe a general stacked-membrane system in the absence of non-uniform flow is given in Fig. 4. Since the response of each component to a unit impulse is well known, convolution of successive linear elements using a Green's function approach [51] is an appropriate method to obtain scaled analytical expressions h_F and h_R which describe forward and reverse-flow experiments, respectively.

In forward flow, convolution of the two extracolumn CSTRs yields $c(t) = [\exp(-t/\tau_r) - \exp(-t/\tau_f)]/(\tau_r - \tau_f)$. The response of the complete system is independent of the order in which its elements are analyzed. It is:

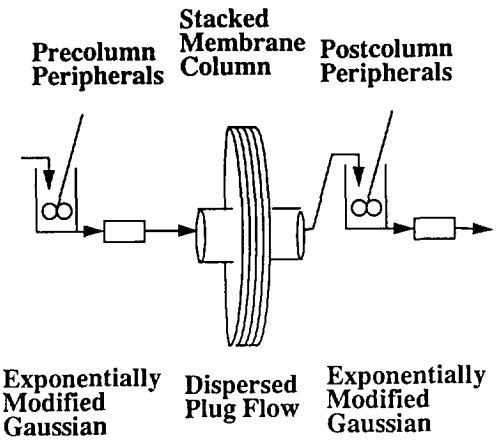

Fig. 4. Conceptual representation of a stacked-membrane column system. Exponentially modified Gaussians (EMGs) account for extracolumn contributions to effluent broadening. EMGs consist of a continuously stirred tank reactor in series with a dispersed plug flow column. The stacked membrane is described by dispersed plug flow in the absence of non-uniform flow.

$$h_F(t) = \frac{1}{2(\tau_r - \tau_f)} \cdot \left\{ \exp\left[\frac{-\sigma_c}{\tau_r} \cdot \left(z_r + \frac{\sigma_c}{2\tau_r} \right) \right] \cdot \left[1 + \mathrm{erf}\left(\frac{z_r}{\sqrt{2}} \right) \right] \right\} - \frac{1}{2(\tau_r - \tau_f)} \cdot \left\{ \exp\left[\frac{-\sigma_c}{\tau_f} \cdot \left(z_f + \frac{\sigma_c}{2\tau_f} \right) \right] \cdot \left[1 + \mathrm{erf}\left(\frac{z_f}{\sqrt{2}} \right) \right] \right\} \quad (3)$$

where subscripts r and f denote the precolumn and postcolumn peripherals. Dimensionless times z_r and z_f are analogues: $z_r \equiv (t - \bar{t}_c)/\sigma_c - \sigma_c/\tau_f$. The composite residence time $\bar{t}_c$ and variance σ_c are sums of the respective moments of the three plug flow reactors: $\bar{t}_c \equiv \bar{t} + \bar{t}_r + \bar{t}_f$ and $\sigma_c^2 = \sigma^2 + \sigma_r^2 + \sigma_f^2$.

The reversed-flow result is obtained in an analogous fashion after reversing the precolumn

peripherals [45]. It is:

$$h_R(t) = \frac{1}{2(\tau_r + \tau_f)} \cdot \left\{ \exp\left[\frac{\sigma_c}{\tau_r} \cdot \left(T + \frac{\sigma_c}{2\tau_r} \right) \right] \cdot \left[\operatorname{erf}\left(\frac{T + \frac{\sigma_c}{\tau_r} + \frac{5\tau_r}{\sigma_c}}{\sqrt{2}} \right) - \operatorname{erf}\left(\frac{T + \frac{\sigma_c}{\tau_r}}{\sqrt{2}} \right) \right] \right\} + \frac{1}{2(\tau_r + \tau_f)} \cdot \left\{ \exp\left[\frac{-\sigma_c}{\tau_f} \cdot \left(T - \frac{\sigma_c}{2\tau_f} \right) \right] \cdot \left[1 + \operatorname{erf}\left(\frac{T - \frac{\sigma_c}{\tau_f}}{\sqrt{2}} \right) \right] \right\} \quad (4)$$

where scaled time $T \equiv (t - \bar{t}_c)/\sigma_c$ and composite residence time and variance are defined as before.

We now summarize our characterization of stacked-membrane performance using the reversed-flow experiment and its analytical description.

3. Experimental

3.1. Materials

All chemicals used were reagent grade except as noted. Two proteins, beef heart cytochrome *c* (Sigma, Type V-A, No. C-2037) and horse heart cytochrome *c* (Sigma, Type II-S, No. C-8266, practical grade) were dissolved at 2.5 mg/ml in 0.02 *M* sodium citrate (Sigma) and 0.5 *M* sodium chloride (Johnson Matthey) at pH 8.0 or buffered to pH 6.0 with hydrochloric acid (Fisher). Solutions were prepared with 18 MΩ distilled, deionized water. Buffers were filtered (0.2 μm) and degassed by vacuum prior to each experimental period.

3.2. Apparatus

Two stacked-membrane columns were analyzed: a 5 mm $L \times 17.17$ mm I.D. Millipore MemSep 1000 DEAE (Bedford, MA, USA) with 1.4 ml nominal bed volume and a 5 mm $L \times 12.7$ mm I.D. Millipore MemSep HP500 DEAE with 0.64 ml nominal bed volume. Forty microporous ($d_p = 1.2$ μm) membranes made from pure regenerated cellulose are stacked in each column for which a uniform matrix porosity ϵ_b 0.827 has been reported [8]. The MemSep 1000 cartridge is rigid polypropylene rated to 7 bar backpressure with recommended volumetric flow-rates between 1.5 and 6 ml/min. The MemSep HP500 cartridge is rigid polyphenylenesulfate rated to 1000 p.s.i. (1 p.s.i. = 6894.76 Pa) and flow-rates between 0.5 and 5 ml/min.

The MemSep 1000 has channels etched into the upper endcap and lower base of the cartridge to distribute and collect the fluid, respectively. There are six evenly spaced channels with semicircular cross-section radiating outward from the fluid inlet. At flow-rates ≤20 ml/min, the channel Reynolds number based on its hydraulic radius, R_h, is <600, suggesting laminar flow. Polypropylene mesh distributors separate the distributors from the membrane stack. Polyethylene seals prevent fluid from pooling near the corners of the bed volume. Bypassing is discouraged by nine exclusion gaskets inserted between every four membranes. Construction of the MemSep HP500 is similar except eight radial distributor arms are connected by about ten concentric grooves of increasing diameter. An antijetting disc is centered beneath the inlet.

Experiments were performed with a Millipore ConSep LC100. From upstream to downstream this system included proportioning valve, gear pump, pressure transducer, UV detector used at 280 nm, and keypad programmer. The ConSep septum injector was replaced by a syringe loading sample injector, Rheodyne Model 7125 (Cotati, CA, USA) equipped with a 20-μl sample loop. The stacked membrane was connected to a Rheodyne Model 7010 injection valve in order to reverse the flow direction. The valves

and column were configured so that precolumn and postcolumn peripherals would have identical lengths and volumes in either forward or reversed flow. A buffer bypass line inserted via a tee between the injection valves and the pressure transducer via a tee dissipated backpressure spikes observed during injection and flow reversal.

Precolumn peripherals included the 20-μl sample loop, 23 cm of 0.02 in. I.D. polyether ether ketone (PEEK) tubing (1 in. = 2.54 cm), luer-lock adaptors for the MemSep 1000, and four ports (two sections) of an injection valve (>67 μl total). Postcolumn peripherals included 13 cm of 0.02 in. and 6 cm of 0.01 in. I.D. PEEK tubing, two ports (one section) of an injection valve, and the detector volume (>29 μl total).

3.3. Procedures

Each column was equilibrated at approximately 1 ml/min in high-ionic-strength buffer before proceeding. Two hours of equilibration were required to regain a stable baseline if buffers were changed. This time corresponds to the time necessary for a small solute to diffuse from the periphery of the column through the intergasket space to the membrane bed to be washed out.

Effluent profiles from precolumn and postcolumn tubing at each flow-rate was measured by plumbing the respective sections between the sample loop and the detector. A 20-μl volume of either 2.5 or 1.25 mg/ml protein was injected to obtain three repetitions. Three repetitions of each column effluent profile were obtained similarly with the column inserted between upstream and downstream peripherals. Flow direction in the reversed-flow runs was changed instantaneously at one-half the peak run time of the corresponding forward-flow experiment.

3.4. Data analysis

Data were acquired on an IBM PS/2 Model 70 386 with Gilson 712 software (Middleton, WI, USA). Data analysis on an IBM PS/ValuePoint 466DX2/D used Microsoft Excel Version 4.0 and an equation solver, EES (Middleton, WI, USA): analysis on a Digital Vaxstation 3100 used Fortran 77 programs.

Extracolumn effluents were fitted to an EMG function using the method of Jeansonne and Foley [50] on the Vaxstation to obtain values of τ and σ for each condition. EES was used to solve implicitly for a corresponding t at the point where the EMG peak intersects its underlying Gaussian. Reversed-flow effluents from the MemSep 1000 and MemSep HP500 were fitted iteratively with Excel to Eq. 3 using averaged extracolumn τ values to obtain $\bar{t}_c$ and σ_c for dispersion in the stack. Peak values larger than half-height were weighted heavier to avoid noise from the tails.

Plate heights were calculated as $L\sigma^2/\bar{t}_c^2$, neglecting residence times of the underlying Gaussian in the peripherals. Reported plate heights are averages of four replicates except for a value at 2 ml/min for the MemSep 1000 (three replicates) and a value at 1 ml/min for the MemSep HP500 (two replicates). Standard deviations of MemSep 1000 plate heights were $<4\%$ of the respective values. Higher deviations for MemSep HP500 occurred as estimated σ_c values were not much larger than σ_r and σ_f: 29% at 0.5 ml/min; 28% at 1 ml/min; 61% at 2 ml/min; and 49% at 4 ml/min.

4. Results and discussion

We begin this discussion by evaluating qualitative effects of extracolumn volumes and nonuniform flow on reversed-flow and forward-flow effluent profiles, respectively. We quantitatively compare reversed-flow analysis of stacked-membrane plate heights with methods based on moments and measured curve widths. And we examine the implications of measured plate heights in MemSep stacked membranes on our one-dimensional dispersive description.

A sample reversed-flow effluent profile obtained as noted above from a MemSep 1000 is compared in Fig. 5 with a fit of Eq. 3. Asymmetry and tailing along the leading edge of the data are greater than those along its trailing edge. This corresponds to larger stirred-tank

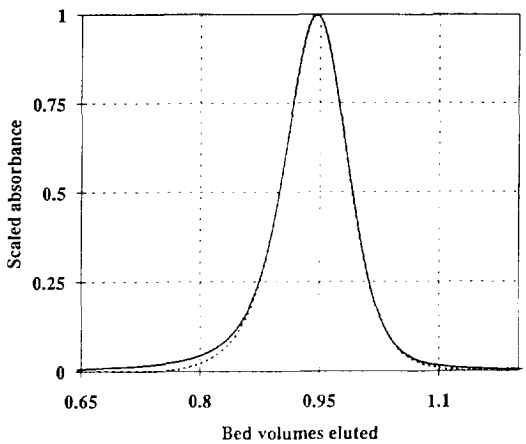

Fig. 5. Comparison of a reversed-flow stacked-membrane effluent shape (solid line) with a fit (dashed line) based on Eq. 3. A 20-μl sample of 2.5 mg/ml cytochrome c was injected into a MemSep 1000 at 2 ml/min for 0.34 min after which the flow direction was reversed. Absorbance at 280 nm was measured across a 10-mm pathlength. Parameter values estimated were the composite mean residence time, $\bar{t}_c$ = 0.664 min and standard deviation σ_c = 0.0175 min.

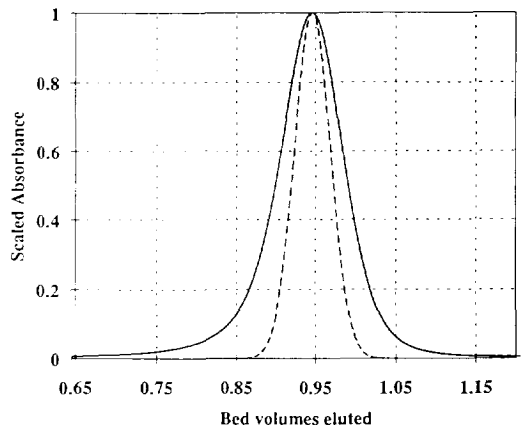

Fig. 6. Comparison of the reversed-flow stacked-membrane effluent profile (solid line) described in Fig. 5 with the Gaussian profile (dashed line) attributed to convective dispersion in the stacked membrane. The Gaussian width at 60.6% of peak maximum, 0.0317 min, was obtained by subtracting variances of precolumn ($\sigma_r^2 = 3.21 \cdot 10^{-5}$ min^2) and postcolumn ($\sigma_t^2 = 2.34 \cdot 10^{-5}$ min^2) peripherals from the composite fitted variance. The data bandwidth at 60.6% of peak maximum was 1.7 × larger than this.

(τ_r = 0.0228 min) and dispersion (σ_r = 0.00566 min) constants in the precolumn peripherals compared with those (τ_t = 0.0185 min, σ_t = 0.00484 min) in postcolumn tubing. Both leading and trailing edges are well matched by the description. (Note that stirred-tank time constants for precolumn and postcolumn peripherals were similar to corresponding space times, V/Q, calculated from peripheral volumes described in Section 3.)

The magnitude of extracolumn contributions to effluent broadening of a stacked-membrane system is illustrated in Fig. 6. The effluent width is 1.7 times that of the convective-dispersion broadening in the stacked membrane. A stacked-membrane plate height estimated from the width at 60.6% peak maximum would have been three times too large. Mistaking this profile for a Gaussian, and neglecting the influence of extracolumn broadening would substantially overestimate stacked-membrane plate heights.

Parameters obtained from extracolumn and reversed-flow experiments allow a priori prediction of forward-flow profiles in the absence of non-uniform flow with Eq. 3. Fig. 7 contrasts the

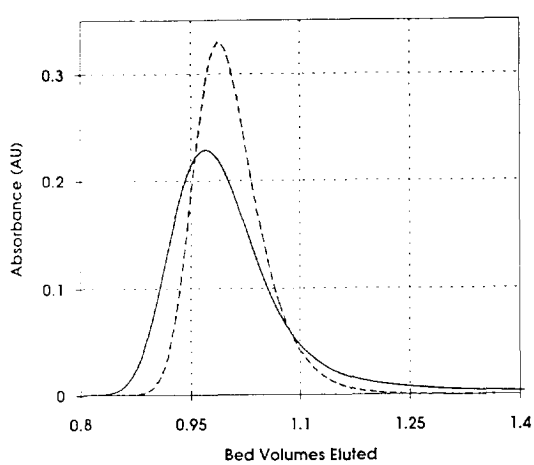

Fig. 7. Comparison of a forward-flow stacked-membrane effluent shape (solid line) with an a priori prediction from Eq. 3 (dashed line) based on parameters obtained from separate experiments. The effluent resulted from a 20-μl sample of 2.5 mg/ml cytochrome c eluted from a MemSep 1000 at 2 ml/min; absorbance at 280 nm was measured across a 10-mm pathlength. Extracolumn stirred-tank time constants, τ_r = 0.0228 min and τ_t = 0.0185 min, were obtained by fitting the respective peripheral effluent profiles to an EMG. Composite residence time, $\bar{t}_c$ = 0.664 min, and standard deviation, σ_c = 0.0175 min, were obtained from a 2 ml/min reverse-flow effluent.

expected peak with the experimentally observed data. Additional broadening in the data arises from non-uniform flow. The most notable consequences of non-uniform flow are (1) severe tailing to 1.94 min and (2) 30% decrease in peak amplitude. Note that the forward-flow prediction in Fig. 7 tails more than its reversed-flow complement in Fig. 6.

Ignoring the effects of non-uniform flow and extracolumn volumes on effluent profiles causes overestimation of stacked-membrane plate heights. The variance of the forward-flow data in Fig. 7 obtained by the experimental method of moments —0.0152 min^2— is 61 times larger than the variance attributable to dispersion in the stacked membrane. Using moments analysis of forward-flow data to estimate plate height as $H \approx L(\langle t^2 \rangle - \langle t \rangle^2)/\langle t \rangle^2$ overestimates stacked-membrane values by orders of magnitude. A "plate height" calculated from the peak width of the forward-flow data in Fig. 7 —0.079 min— is 6.2 times the reversed-flow estimate.

Plate heights estimated for MemSep stacked membranes from reversed-flow experiments are summarized together with predictions from dispersive theory in Fig. 8. These values, ca. 10 times lower than previous reports, are within a factor of three of the theory and tend to decrease with increasing velocity.

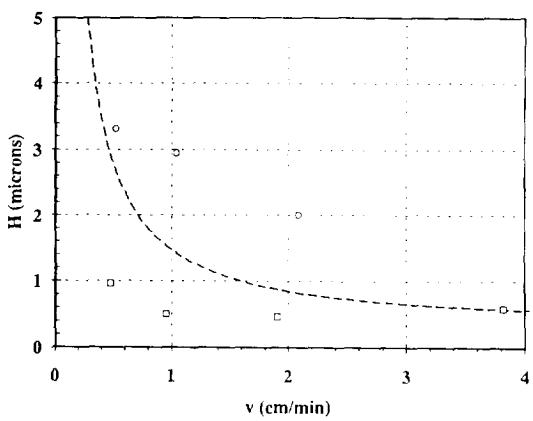

Fig. 8. Plate heigths estimated for a MemSep 1000 (○) at 1, 2 and 4 ml/min and for a MemSep HP500 (□) at 0.5, 1, 2 and 4 ml/min. Respective reversed-flow effluents from a 20-μl injection of 2.5 mg/ml cytochrome *c* were fitted to Eq. 3. Corresponding theoretical plate heights due to convective dispersion, $H = 2\epsilon/v$ (dashed line) were calculated from ϵ in Eq. 2 using $D_f = 11.4 \cdot 10^{-7}$ cm^2/s [52], $D_p = 1.883 \cdot 10^{-4}$ cm, and $\epsilon_b = 0.827$.

In a 5-mm column, the corresponding number of theoretical plates ranges from about 1500 at 0.5 cm/min to a maximum of 10 900 at 2 cm/min. This justifies using a long-column approximation in Eqs. 3 and 4 to describe the stacked membrane. Dispersion along streamlines whose velocities vary from the mean will not differ appreciably in forward or reversed flow because (1) the range of operational stacked-membrane velocities gives approximately the same dispersion (the Van Deemter slope is flat) and (2) the number of stages is high. Profiles from differing streamlines are nearly superimposable in the absence of non-uniform flow, and may be efficiently treated by a one-dimensional description.

Our examination of transport in stacked-membrane systems suggests: (1) reversed-flow analysis measures stacked-membrane plate height more accurately than methods based on moments or peak width, particularly when effects of extracolumn volumes and non-uniform flow on effluent profiles are large; (2) dispersive stacked-membrane plate heights are on the order of a micrometer; (3) both the magnitude and trend of stacked-membrane plate heights estimated by reversing the flow are consistent with intuitive and theoretical estimates of convective dispersion in porous beds.

We have been careful to distinguish between dispersive broadening, and mechanical broadening due to a distribution of residence times. While these processes are physically and mathematically distinct, their common effect, where present, is to diminish the ability to separate efficiently. In spite of apparent flow non-uniformity, commercially available stacked membranes are suitable for analytical separations in which a small percentage of severe tailing is manageable. Careful selection of peripherals to minimize extracolumn broadening (especially downstream of the column) will enhance their performance. For preparative separations in which rapid regeneration, cleanability, and high purity are required, non-uniform flow may hinder the applicability of stacked membranes.

Comparing forward- and reversed-flow results to select an aspect ratio, distributor, or exclusion device to minimize flow non-uniformity in large-scale devices appears useful.

The intrinsic separation potential of stacked membranes which we have measured appears large enough to justify efforts to improve their design. They are, for example, interesting candidates for subunits in Sorbex-type simulated-moving-bed separations. The extremely low solid-phase requirement in moving beds, relative to fixed-bed chromatography, would not demand large membrane capacities. In such a system, low pressure drop, rapid "particle" response times, and low volumetric holdups characteristic of membranes would allow a broader selection of operating conditions while decreasing the demand for high pressure peripherals.

Symbols

Alphanumeric symbols

- A column cross-sectional area (cm^2)
- b length of unit cell (cm)
- c width of unit cell (cm)
- c_f solute concentration in moving fluid phase in chromatography (g/cm^3)
- d width of unit-cell inlet (cm)
- d_p pore diameter in membrane (cm)
- D_f effective solute diffusivity in free solution (cm^2/s)
- D_p effective particle diameter in packed bed (cm)
- h system response to a unit impulse
- H height equivalent to a theoretical chromatographic plate (cm)
- L length of chromatographic column ($=HN$) (cm)
- m_0 total solute mass which enters chromatography column in a pulse (g)
- N number of stages or column plates
- Pe dispersion Peclet number ($\equiv vD_p/\epsilon$)
- Q flow-rate (cm^3/min)
- Re Reynolds number ($\equiv D_p v \epsilon_b/\nu$)
- s standard deviation
- Sc Schmidt number ($\equiv \nu/D_f$)
- t time (s)
- $\bar{t}$ mean residence time in chromatography (s)
- u equilibrium fraction of a species in the fluid phase
- v interstitial velocity in chromatography, velocity in a unit cell (cm/s)
- V volume (cm^3)
- z axial coordinate (cm)
- z_0 mean position of a solute peak at a given time, defined as uvt (cm)

Greek letters

- α_i partition coefficient of a solute between fluid and solid phase
- ϵ convective axial dispersion coefficient (cm^2/s)
- ϵ_b interparticle or column void volume
- ν kinematic viscosity ($\equiv \mu/\rho$) (cm^2/s)
- Φ velocity potential function (cm^2/s)
- Ψ stream function (cm^2/s)
- σ standard deviation (s)
- τ characteristic time (s)

Subscripts and superscripts

- b bulk (stationary) phase in chromatography
- c composite
- f postcolumn peripherals
- F forward flow
- p phase identification subscript
- r precolumn peripherals
- R reversed flow

References

[1] C. Horvath, *GEN*, 14, No. 9 (1994) 4.
[2] R.E. Majors, *LC·GC*, 12 (1994) 278.
[3] E.L. Paul and C.B. Rosas, *Chem. Eng. Progr.*, 12 (1990) 17–25.
[4] V.B. Lawlis and H. Heinsohn, *LC·GC*, 11 (1993) 720–729.
[5] N.B. Afeyan, N.F. Gordon, L. Mazsaroff, L. Varady, S.P. Fulton, Y.B. Yang and F.E. Regnier, *J. Chromatogr.*, 519 (1990) 1–29.
[6] S. Fulton et al., *Biotechn.*, 12 (1992) 742–747.
[7] A. Depalma, *GEN*, 13, No. 1 (1993) 15.
[8] M.S. Le and J.L. Sanderson, *US Pat.*, 4 895 806 (1990).

[9] F. Svec, presented at the *PrepTech94 Industrial Separations Technology Conference, Secaucus, NJ, 22–24 March 1994.*
[10] D.M. Ruthven and C.B. Ching, *Chem. Eng. Sci.*, 44 (1989) 1011–1038.
[11] D.K. Roper and E.N. Lightfoot, *J. Chromatogr. A*, 654 (1993) 1–16.
[12] A. Seidel-Morgenstern and G. Guiochon, *AIChE J.*, 39 (1993) 809–819.
[13] K.-G. Briefs and M.-R. Kula, *Chem. Eng. Sci.*, 47 (1992) 141–149.
[14] X. Zhang, R.D. Whitley and N.-H.L. Wang, presented at the *AIChE Annual Meeting, Los Angeles, CA, 17–22 November 1991.*
[15] P. Schadle, presented at *PrepTech94, Industrial Separations Technology Conference, Secaucus, NJ, 22–24 March 1994.*
[16] S.-Y. Suen and M.R. Etzel, *Chem. Eng. Sci.*, 47 (1992) 1355–1364.
[17] J.L. Coffman, D.K. Roper and E.N. Lightfoot, *Bioseparation*, 4 (1994) 183–200.
[18] D. Josić, J. Reusch, K. Löster, O. Baum and W. Reutter, *J. Chromatogr.*, 590 (1992) 59–76.
[19] J.A. Gerstner, R. Hamilton and S.J. Cramer, *J. Chromatogr.*, 596 (1992) 173–180.
[20] J.J. van Deemter, F.H. Zuiderweg and A. Klinkenberg, *Chem. Eng. Sci.*, 5 (1956) 271–289.
[21] E. Glueckauf, *Trans. Farad. Soc.*, 51 (1955) 34–44.
[22] A. Klinkenberg and F. Sjenitzer, *Chem. Eng. Sci.*, 5 (1956) 258–270.
[23] L.R. Snyder, in Cs. Horváth (Editor), *High-Performance Liquid Chromatography —Advances and Perspectives*, Vol. 1, Academic Press, New York, 1980, pp. 207–316.
[24] J.C. Giddings, *Unified Separation Science*, Wiley, New York, 1991.
[25] A.M. Lenhoff, *J. Chromatogr.*, 384 (1987) 285–299.
[26] A.M. Athalye, S.J. Gibbs and E.N. Lightfoot, *J. Chromatogr.*, 589 (1992) 71–85.
[27] D.D. Frey, R. Van de Water and B. Zhang, *J. Chromatogr.*, 603 (1992) 43–47.
[28] S. Yamamoto and Y. Sano, *J. Chromatogr.*, 597 (1992) 173–179.
[29] H.C. Liu and J.R. Fried, *AIChE J.*, 40 (1994) 40–49.
[30] R.B. Bird, W.E. Stewart and E.N. Lightfoot, *Transport Phenomena*, Wiley, New York, 1960.
[31] R. Aris and N.R. Amundson, *Mathematical Methods in Chemical Engineering*, Prentice Hall, Englewood Cliffs, NJ, 1973.
[32] E.N. Lightfoot, S.J. Gibbs, A.M. Athalye and T.H. Scholten, *Isr. J. Chem.*, 30 (1990) 229–237.
[33] D.M. Ruthven, *Principles of Adsorption and Adsorption Processes*, Wiley-Interscience, New York, 1984.
[34] H.C. Thomas, *J. Am. Chem. Soc.*, 66 (1944) 1664–1666.
[35] S.J. Gibbs and E.N. Lightfoot, *Ind. Eng. Chem. Fundam.*, 25 (1986) 490–498.
[36] F.D. Antia and Cs. Horváth, *J. Chromatogr.*, 484 (1989) 1–27.
[37] A.M. Athalye, *Ph.D. Thesis*, University of Wisconsin, Madison, WI, 1994.
[38] J.F.G. Reis et al., *Sep. Sci. Technol.*, 14 (1979) 367–394.
[39] M.A. Northrup et al., *Chem. Eng. Sci.*, 48 (1993) 13–23.
[40] D.L. Koch and J.F. Brady, *J. Fluid Mech.*, 154 (1985) 399–427.
[41] F. Balzereit, *M.S. Thesis*, University of Wisconsin, Madison, WI, 1991.
[42] K.R. Raths, *M.S. Thesis*, University of Wisconsin, Madison, WI, 1992.
[43] L.M. Milne-Thompson, *Theoretical Hydrodynamics*, Macmillan, London, 5th ed., 1967.
[44] D.K. Roper and E.N. Lightfoot, presented at the *AIChE Annual Meeting, St. Louis, MO, 7–12 November 1993.*
[45] D.K. Roper and E.N. Lightfoot, *Chem. Eng. Sci.*, 49 (1994) 1621–1630.
[46] J.S. Vrentas and C.M. Vrentas, *AIChE J.*, 34 (1988) 1423–1430.
[47] Ph. Daskopolous and A.M. Lenhoff, *AIChE J.*, 34 (1988) 1423–1430.
[48] K.P. Mayock, J.M. Tarbell and J.L. Duda, *Sep. Sci. Technol.*, 15 (1980) 1285–1296.
[49] T. Korenaga, F. Shen and T. Takahashi, *AIChE J.*, 35 (1989) 1395–1398.
[50] M.S. Jeansonne and J.P. Foley, *J. Chromatogr.*, 594 (1992) 1–8.
[51] I. Stakgold, *Greens Functions and Boundary Value Problems*, Wiley, New York, 1979.
[52] M.T. Tyn and T.W. Gusek, *Biotechnol. Bioeng.*, 35 (1990) 327–338.